Electrochemical Synthesis of Urea: Co-reduction of Nitric Oxide and Carbon Monoxide

Hao Wan,[†] Xingli Wang,[‡] Lei Tan,[‡] Michael Filippi,[‡] Peter Strasser,[‡] Jan Rossmeisl,[†] and Alexander Bagger[*,†,¶]

[†]*Center for High Entropy Alloy Catalysis (CHEAC), Department of Chemistry, University of Copenhagen, Universitetsparken 5, DK-2100 Copenhagen, Denmark*

[‡]*Department of Chemistry, Chemical Engineering Division, Technical University Berlin, 10623 Berlin, Germany*

[¶]*Department of Chemical Engineering, Imperial College London, 2.03b, Royal School of Mines, Prince Consort Rd, London SW7 2AZ, England*

E-mail: Alexander@chem.ku.dk

Abstract

Electrocatalytic conversion is a promising technology for storing renewable electricity in the chemical form. Substantial efforts have been made on the multi-carbon feedstock production, while producing nitrogen-containing chemicals like urea via C-N coupling little is known. Here, we elucidate the possible urea production on metals through co-reduction of nitric oxide (NO) and carbon oxide (CO). Based on adsorption energies calculated by DFT, we find that Cu is able to bind both ∗NO and ∗CO while not binding ∗H. During NO + CO co-reduction, we identify two kinetically and thermodynamically possible C-N couplings via ∗CO + ∗N and ∗CONH + ∗N, and further

hydrogenation leads to urea formation. A 2-D activity heatmap has been constructed for describing nitrogen conversion to urea. This work provides a clear example of using computational simulations to predict selective and active materials for urea production.

Keywords

DFT Simulations, Electrocatalysis, C-N coupling, NO_x Removal, Urea Synthesis

The electroreduction of CO_2 is a promising technology for carbon utilization. In the electrolysis of CO_2 or CO_2-derived CO, most efforts have been devoted to promoting C-C bond formation to generate important industrial multi-carbon feedstock such as ethylene, ethanol, n-propanol and acetate. However, bonding the C atom of CO_2 with other valuable heteroatoms (e.g., N) is an alternative strategy to produce value-added products which is highly beneficial for expanding the application of CO_2RR.[1–3]

N-containing chemicals, such as urea, amides, amines, and nitriles, are of widespread importance for the bulk chemicals, synthetic intermediates, fertilizers, agrochemicals, and pharmaceuticals.[4–6] Currently, the synthesis of these molecules is all dominated by thermocatalytic transformation of NH_3 precursors under harsh conditions.[3] Especially, the production of urea (NH_2CONH_2) consumes approximately 80% of the global NH_3.[7–9] In principle, the formation of C-N bonds for urea should be possible mixing CO_2 or CO with nitrogen species (NO_x), like NO_3^-, NO_2^- and NO, when suitable catalysts are utilized.[10,11] Nevertheless, the formidable challenge is that the direct electroreduction of CO_2 or NO_x to single carbon or nitrogen species competes with the urea formation. This results in a complex products distribution with low Faradaic efficiency (FE) of urea and also with a need for product separation.[12]

The concept of electrocatalytic co-reduction of CO_2 and NO_x was to the best of our knowledge tested in 1995 by Shibata *et al.* to produce urea[13] and more recently has gained interest in the community.[14] The product distribution as a function of potential, as mea-

sured by Shibata *et al.* with a Cu loaded gas-diffusion electrode (GDE), is shown in Fig. 1.[13,15,16] With simultaneous reduction of CO_2 + NO_3^- (Fig. 1(a)) or CO_2 + NO_2^- (Fig. 1(b)), the observed dominant product in both experiments from CO_2 reduction in this GDE setup is CO, which increases with increasing the overpotential. Note that today, research groups report high hydrocarbon production and FE from Cu electrode in GDE.[17,18] For NH_3 and urea formation, similar current efficiency trend is observed and it decreases with increasing the overpotential. At potential of -0.25 V vs. RHE (reversible hydrogen electrode), the current efficiency of urea with approximately 37% was obtained for CO_2 + NO_2^- co-reduction.[13] However, the absolute current for each product was not reported. Besides, experimentally, the detection of urea in presence of NO_x species usually involves a two-step process, in which urea is firstly decomposed by ureases into ammonia, and then the amount of ammonia measured by spectrophotometer.[15,16] The pre-quantification of ammonia is thus crucial, since ammonia is also the product of direct reduction of NO_x. In another word, a rigorous protocol for experimental urea detection is highly demanded.

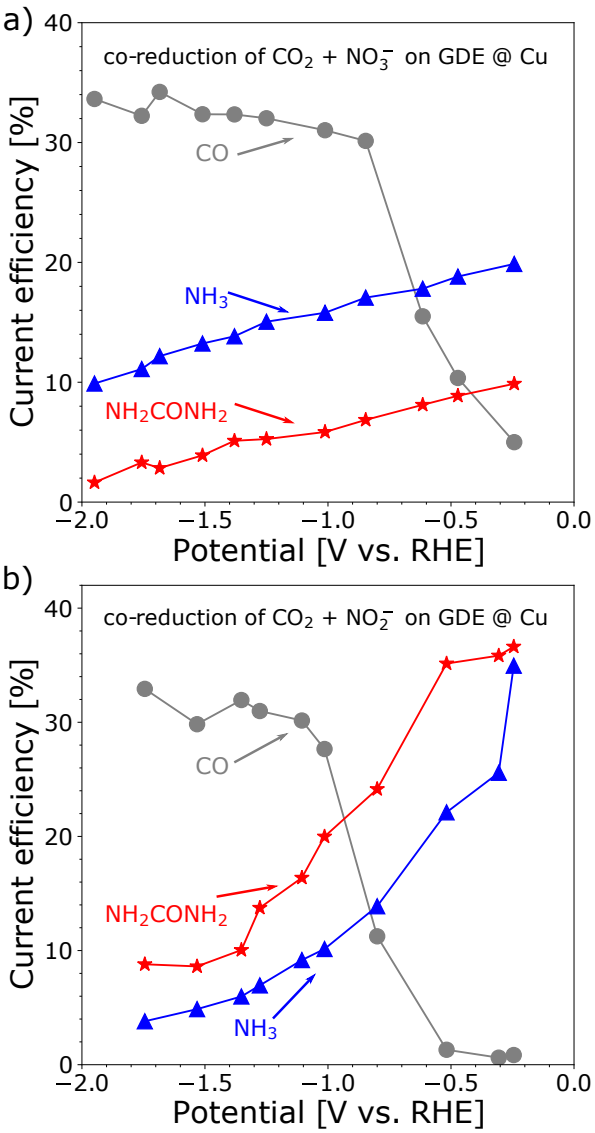

Figure 1: Experimentally determined major product distribution (current efficiency) from electrocatalytic (a) co-reduction of CO_2 + NO_3^- and (b) co-reduction of CO_2 + NO_2^- at a Cu loaded gas-diffusion electrode (GDE) as a function of electrode potential (versus reversible hydrogen electrode, RHE), as measured by Shibata *et al.*[13,15,16]

Cu-based materials represent as an important category of electrochemical CO_2 reduction catalysts, allowing the production of hydrocarbons with adsorbed CO as a key intermediate.[19,20] Furthermore, Cu-based electrocatalysts have been investigated for electrochemcial reduction of nitrogen species (NO_x) with high FE (greater than 90%) for NH_3 formation.[21–24] For electrocatalytic NO_3^-/NO_2^- reduction, adsorbed nitric oxide ($*NO$, $*$ denotes the active site.) has been suggested as a divergent center, which may control the electrocatalytic

selectivity towards NH_3 production.[24–30] As a result, electrochemical NO reduction might provide a more sufficient way for NH_3 formation.[25–28,31]

In this work, we investigate the C-N couplings for urea formation during the electrocatalytic co-reduction of NO + CO among a group of metals via density functional theory (DFT) simulations. The co-reduction of NO + CO provides a study model for understanding the fundamentals of electrocatalytic C-N coupling reactions, developing amides or more specifically, sufficient urea production technologies. The classification mapping has been previously utilized to understand the selectivity on metals for CO[32,33] and NO reduction[24] with two descriptors. Cu is the only metal that binds both $*$NO and $*$CO molecules, but but does not have a strong affinity to $*H_{UPD}$ (under potential deposited $*$H). Essentially meaning that Cu has a lower coverage of $*$H at reduction conditions allowing CO and NO reduction to take place relatively efficiently. Utilizing this knowledge, we investigate the selectivity during co-reduction of NO + CO, by possible C-N couplings for urea production. We simulate activation barriers for C-N couplings, and construct a 2-D activity heatmap for describing nitrogen conversion towards urea.

In the electrochemical co-reduction of NO + CO, multiple reactions are possible. Here, we list four important ones:

$$2\,(H^+ + e^-) \longrightarrow H_2 \qquad E^0 = 0.0\,V \qquad (1)$$

$$CO + 6\,(H^+ + e^-) \longrightarrow CH_4 + H_2O \qquad E^0 = 0.26\,V \qquad (2)$$

$$NO + 5\,(H^+ + e^-) \longrightarrow NH_3 + H_2O \qquad E^0 = 0.71\,V \qquad (3)$$

$$CO + 2\,NO + 8\,(H^+ + e^-) \longrightarrow NH_2CONH_2 + 2\,H_2O \qquad E^0 = 0.92\,V \qquad (4)$$

For each reaction, the standard reduction potential *versus* RHE is shown on the right. Thermodynamically, urea formation has the highest equilibrium potential, which should result in a large driving force for urea. However, due to the existence of overpotential and the large amount of proton electron transfers, the other reactions are still competitive. With

aim to conduct electrocatalytic NO + CO reduction on catalysts, both NO and CO species are expected to be adsorbed on the surfaces. In addition, the competition from hydrogen evolution reaction (HER) also has to be avoided at negative potentials.

Fig. 2(a) shows the classification scheme[32] of adsorption energies of ∗CO plotted against ∗H adsorption energy. The horizontal line in Fig. 2(a) shows the equilibrium between CO gas and adsorbed ∗CO while the vertical line depicts the equilibrium between $(1/2)H_2$ and adsorbed ∗H under standard conditions. The blue dotted line describes the linear fitting between ∗CO and ∗H adsorption energies of transition metals, except metals from group 12 and above which do not bind ∗CO and hence these values are much too low as compared to how their binding in reality is. Note that the crossing point (indicated by (1)) between the linear fit and the vertical line is important.

Fig. 2(b) illustrates the classification scheme[24] of adsorption energies of ∗NO plotted against ∗H adsorption energy. The horizontal line illustrates the equilibrium between NO (gas) and adsorbed ∗NO and the vertical line shows the equilibrium between $(1/2)H_2$ and adsorbed ∗H. The blue dotted line is obtained from the linear fitting between ∗NO and ∗H adsorption energies without including metals from group 12 and above. The crossing point between the linear fit and the vertical line is indicated by (2). In combination, it is found that Cu is the only metal binding both ∗NO and ∗CO but not ∗H below the equilibrium line of $1/2H_2 \leftrightarrow$ ∗H. This could lead to a selective NO + CO reduction. Metals on the left of vertical line (both in Fig. 2(a) and (b)) like Pt, Pd, bind ∗CO , ∗NO and ∗H very strongly, resulting in HER, especially at potential below 0 V vs RHE. For the metals above the horizontal line in 2(b), such as Au or Ag, it is unfavourable to bind ∗CO or ∗NO, which does not allow CO or NO reduction.

Fig. 2(c) presents a direct adsorption energy comparison between ∗NO and ∗CO. The diagonal line in Fig. 2(c) exhibits the equal adsorption strength for ∗NO and ∗CO adsorption. Metals are at or below the diagonal line, indicating that the adsorption of ∗NO is always stronger than ∗CO adsorption. Using the linear fittings of ∗CO vs. ∗H and ∗NO vs. ∗H

in Fig. 2(a) and (b), allows to co-plot two lightblue lines. These two blue lines show the equilibrium between $(1/2)H_2$ and adsorbed $*H$. Metals on the right of vertical blue line (1) and also above the horizontal blue line (2), are required in order to avoid high $*H$ adsorption, and hereby H_2 evolution. Utilizing the information of $*NO$ and $*CO$ binding with the linear fittings, allows the construction of an area where we can classify urea formation for catalysts. As observed, for all metals they lie below the diagonal line showing a preferred stronger binding of NO than CO. This indicates that NO reduction is easier than CO, even without considering the thermodynamic potentials. Here, the urea production area is marked with blue color and for metal catalysts only Cu metal leads to possible urea conversion. Here, it has to be mentioned that the classification analysis is a necessary property to fulfill, but may not be sufficient, to describe urea formation on metal catalysts. In cases where catalysts do not bind $*CO$ and $*NO$ there may still be a minor probability of urea formation as found in the case of about 4.55% urea formation on Zn under H-type cell.[10] Similar observations have been made for CO_2 reduction on Ag, which does not bind $*CO$, but can have minor C-C products turnovers of about 1.17 % at 60 bars.[34]

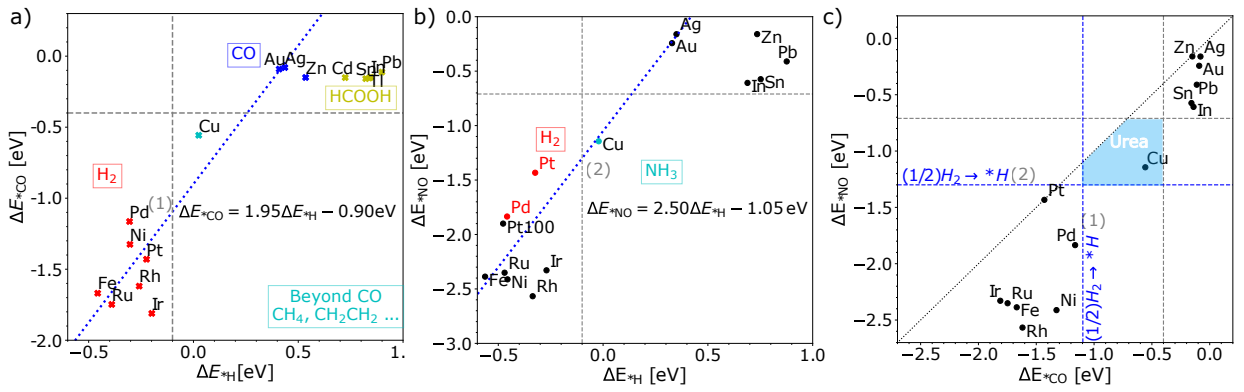

Figure 2: The adsorption energies of the intermediates on metals: (a) ∗CO and ∗H; (b)∗NO and ∗H; (c) ∗CO and ∗NO. The vertical lines in (a) and (b) show the equilibrium between $(1/2)H_2$ and adsorbed ∗H under standard conditions. The horizontal line in (a) exhibits the equilibrium for CO → ∗CO with $\Delta G_{*\mathrm{CO}} = 0$ which is also indicated in the vertical gray line in (c). The horizontal lines in (b) and (c) illustrate the equilibrium for NO → ∗NO with $\Delta G_{*\mathrm{NO}} = 0$ and the diagonal line in (c) shows the equal adsorption strength of ∗CO and ∗NO. Line (1) in (a) describes the linear fitting between ∗CO and ∗H adsorption energies with $\Delta E_{*\mathrm{H}}$ below 0.5 eV. Line (2) in (b) is obtained from the linear fitting between ∗NO and ∗H adsorption energies with $\Delta E_{*\mathrm{H}}$ below 0.5 eV. The lightblue lines in (c) are obtained from scaling relations on ∗CO vs. ∗H (line (1)) and ∗NO vs. ∗H (line (2)). Data is obtained from ref. 24,32,33.

For electrochemical co-reduction of NO + CO, C-N coupling can happen via CO and NO reduction intermediates. Using the observation that ∗NO binds stronger and NO protonation proceeds at lower overpotential than CO protonation,[24,32] we investigate the first C-N bond formation via the coupling between ∗CO and ∗NHO, ∗NOH, ∗NHOH, ∗N, ∗NH, ∗NHH intermediates.

Fig. 3 illustrates the activation barriers (E_a) for C-N bond formation. In Fig. 3(a), the ∗CO + ∗N coupling barrier is plotted against the reaction energies (ΔE). A Brønsted-Evans-Polanyi (BEP) scaling relation between the reaction and transition-state energies for this C-N bond formation is obtained, shown in a dotted line. Au has the lowest barrier whereas Pd or Pt have the highest barrier. The barrier for Cu is between the two extremes. The activation barrier between ∗CO + ∗N on Cu is around 0.50 eV which is acceptable since the rate of 1 s^{-1} can be obtained at the activation barrier of 0.75 eV (gray dashed horizontal line) at room temperature.[35] Furthermore, other C-N couplings between ∗CO and ∗NH_x (x

= 1,2) on Cu are all energetically downhill (Fig. S1) and with an increase in x, the ΔE also increases.

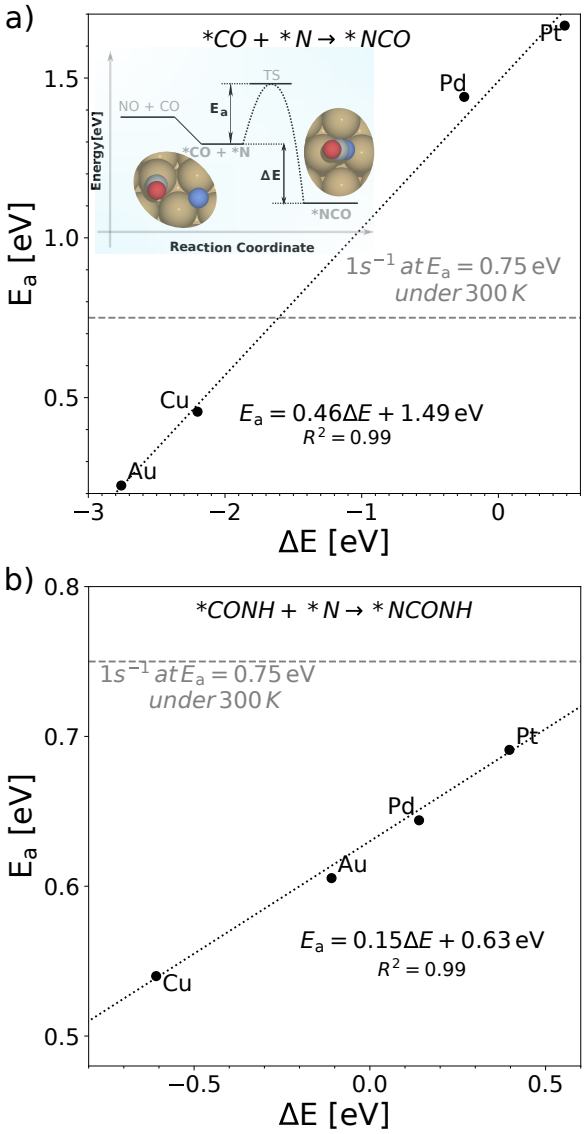

Figure 3: Activation barriers for C-N coupling on (111) facets (a) between ∗CO and ∗N; (b) ∗CONH and ∗N intermediates. Inset in (a) illustrates the energy diagram for ∗CO and ∗N coupling activation on a catalyst. The atomically adsorbed (∗CO + ∗N) and ∗NCO states, as well as the transition state (TS) are indicated. Two Brønsted-Evans-Polanyi (BEP) scaling relations between the reaction and transition-state energies for C-N bond formation are exhibited in dashed lines. The horizontal lines show the activation barrier of 0.75 eV at 300K which provides a rate of 1 s^{-1}.

Fig. 3(b) shows the relation between ∗CONH + ∗N coupling barrier and reaction energy while the second C-N bond formation from ∗CON + ∗N (Fig. S2) is ruled out due to being

a reaction step which is uphill energy. Compared to ∗CO + ∗N coupling, the favorable BEP scaling for ∗CONH + ∗N coupling, indicates its fast kinetics. For Cu, C-N coupling via ∗CONH + ∗N intermediates is energetically downhill while it is unfavourable to form C-N bond for other metals like Au, Pt and Pd. Further urea production is achieved on Cu through continuous hydrogenation of a ∗NCONH intermediate.

The analysis above, suggests possible reaction path for urea formation on Cu during co-reduction of NO + CO. Fig. 4 demonstrates the energy diagram for (a) NO to NH_3, (b) CO to CH_4 and (c) NO + CO towards urea formation. The energy for NO reduction, CO reduction and NO + CO co-reduction is 0.23 eV, 0.52 eV and 0.23 eV respectively. This suggests that NO reduction is more favorable than CO during NO + CO co-reduction process. This data is supported by experimental observations of NO reduction towards NH_3 on Cu starting at 0.3 V vs. RHE[23] and CO reduction to hydrocarbons formation on Cu starting at potential below -0.4 V vs. RHE.[36,37] Furthermore NO and NO + CO reductions share a common limiting potential, making NO reduction and the co-reduction in direct competition - which is also observed in Fig. 1 by these two products having the same behaviour with potential.

Fig. 4(c) presents the reaction path for urea formation from co-reduction of NO + CO via two C-N couplings: (1) ∗CO and ∗N coupling; (2) ∗CONH and ∗N coupling. Three energy uphill steps are identified: (1): hydrogenation of ∗NO is potential dependent with 0.23 eV; (2) and (3): C-N couplings are potential independent and have a barrier with 0.50 eV and 0.52 eV respectively. The hydrogenation of ∗NO is a shared step for NH_3 and urea production, indicating a competition between those two products. Therefore, thermodynamics for C-N and N-H bond formation have been also compared here. A more negative reaction energy for ∗CO and ∗N coupling (-2.23 eV) than ∗N and ∗H coupling (-1.53 eV) provides a higher driving force for C-N bond formation. Second C-N bond formation happens with 0.52 eV energy barrier via coupling between ∗CONH and ∗N intermediates where ∗CONH is formed through the hydrogenation of ∗NCO. Further protonation towards ∗NCONH and ∗NHCONH leads to urea formation. Overall, for C-N bond formation, the first C-N bond

formation can be treated as the rate determining step. This computational analysis above suggests possible explanation for the experimental reports where electrocatalytic C-N coupling is widely observed on Cu-based catalysts with acceptable Faradaic efficiency for amides formation, such as urea.[2,3,13,15,16,38]

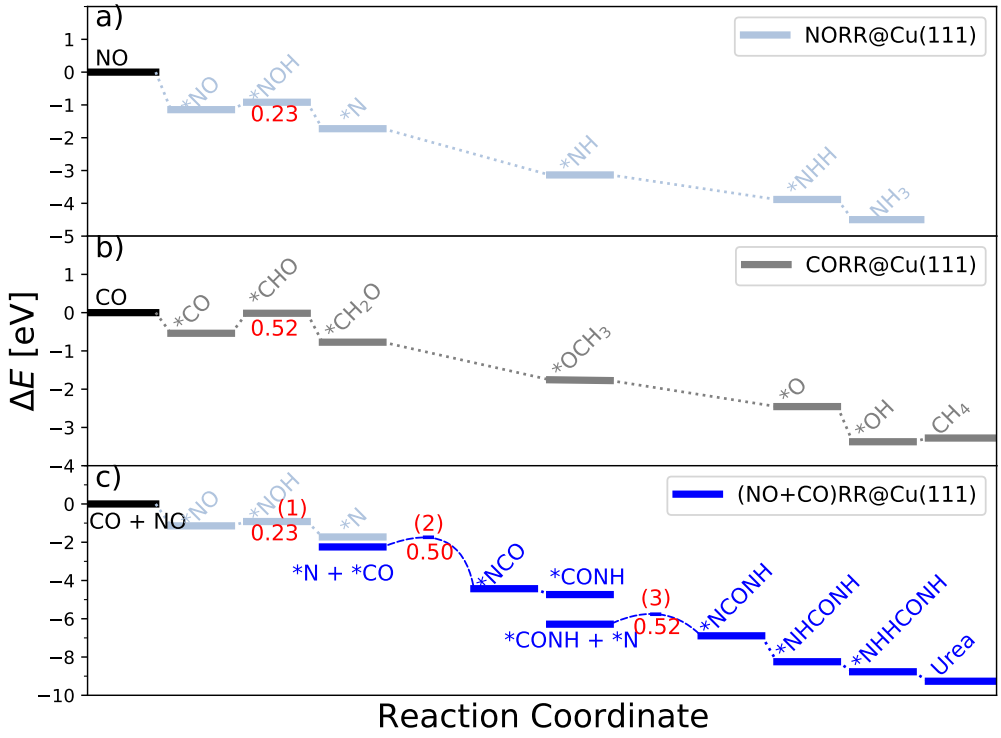

Figure 4: The energy diagram on Cu(111) for (a) NO reduction to NH_3; (b) CO reduction towards CH_4; (c) Co-reduction of NO + CO for urea production with barriers for ∗CO and ∗N coupling and ∗CONH and ∗N coupling considered. This is made without free energy and solvation corrections.

Here, with aim to investigate how to control the reaction towards urea as compared with NH_3 formation, since they are really linked in this process, the efficiency for nitrogen conversion to urea but not the FE for all products in the NO + CO co-reduction has been considered. A 2-D reaction activity heatmap has been constructed for urea formation, where BEP relation from Fig. 3(a) and intermediates scaling relations (Fig. S3) are utilized to reduce the complexity. Further, to keep the microkinetic model simple but still capturing the important chemistry, we consider the following reactions: urea formation with the first

C-N bond formation (∗CO and ∗N coupling) as the rate-determining step (RDS) and for NH_3 formation using the ∗NOH formation as RDS which is potential dependent [24] while the former is not. Here, CO reduction is not included.

$$\mathrm{NO} + * \overset{\mathrm{K_1}}{\longleftrightarrow} * \mathrm{NO} \tag{5}$$

$$* \mathrm{NO} + 2\,\mathrm{H^+} + 2\,\mathrm{e^-} \overset{\mathrm{K_2}}{\longrightarrow} * \mathrm{N} + \mathrm{H_2O} \tag{6}$$

$$\mathrm{CO} + * \overset{\mathrm{K_3}}{\longleftrightarrow} * \mathrm{CO} \tag{7}$$

$$* \mathrm{N} + * \mathrm{CO} \overset{\mathrm{k_4^+}}{\longrightarrow} * \mathrm{NCO} \quad (RDS) \tag{8}$$

$$* \mathrm{NCO} + * \mathrm{N} + 4\,\mathrm{H^+} + 4\,\mathrm{e^-} \longrightarrow 2* + \mathrm{NH_2CONH_2} \tag{9}$$

$$* \mathrm{NO} + \mathrm{H^+} + \mathrm{e^-} \overset{\mathrm{k_6}}{\longrightarrow} * \mathrm{NOH} \quad (RDS) \tag{10}$$

$$* \mathrm{NOH} + 4\,\mathrm{H^+} + 4\,\mathrm{e^-} \longrightarrow * + \mathrm{NH_3} + \mathrm{H_2O} \tag{11}$$

From where we can find that, the analytical expression for the rate (R) in the area where ∗NO and ∗CO adsorbed but not binding ∗H can written as:

$$\mathrm{R_{urea}} = \mathrm{k_4^+ K_1 K_2(U) K_3 P_{NO} P_{CO} P_{H_2O}^{-1}}\, {\theta_*}^2 \tag{12}$$

$$\mathrm{R_{NH_3}} = \mathrm{K_1 k_6(U) P_{NO}} \theta_* \tag{13}$$

$$\text{Nitrogen conversion to Urea} = \mathrm{R_{urea}/(R_{urea} + R_{NH_3})} \times 100\% \tag{14}$$

where $\theta_* = (1 + \mathrm{K_1\ P_{NO}} + \mathrm{K_3\ P_{CO}} + \mathrm{K_1 K_2 P_{NO} P_{H_2O}^{-1}})^{-1}$ and U (vs. RHE) is applied potential.

with

$$\mathrm{K_1} = \exp^{-\frac{\Delta \mathrm{G_{*NO}}}{\mathrm{k_B T}}} \qquad \mathrm{K_2(U)} = \exp^{-\frac{\Delta \mathrm{G_{*N}} - \Delta \mathrm{G_{*NO}} - 2\mathrm{eU}}{\mathrm{k_B T}}}$$

$$\mathrm{K_3} = \exp^{-\frac{\Delta \mathrm{G_{*CO}}}{\mathrm{k_B T}}} \qquad \mathrm{k_4{}^+} = \frac{\mathrm{k_B T}}{\mathrm{h}} \exp^{-\frac{\Delta \mathrm{E_a}}{\mathrm{k_B T}}}$$

$$\mathrm{k_6(U)} = \frac{\mathrm{k_B T}}{\mathrm{h}} \exp^{-\frac{\Delta \mathrm{G_{*NOH}} - \Delta \mathrm{G_{*NO}} - \mathrm{eU}}{\mathrm{k_B T}}}$$

E_a stands for the activation barrier for $*$CO and $*$N coupling (see Fig. 3(a)). Under a certain temperature, pressure of the reactants (P_{NO}, P_{CO}), and applied potential (U), the rate depends exactly on two electronic energy parameters: ΔE_{*CO} and ΔE_{*NO}. Fig. 5 shows the nitrogen conversion to urea ($R_{urea}/(R_{urea} + R_{NH_3}) \times 100$ %) as a function of $*$NO and $*$CO adsorption energies with Eq. 12 and Eq. 13 applied in the area where $*$NO and $*$CO adsorbed but not binding $*$H. The kinetic model is calculated at a temperature of 300K, and Fig. 5(a) and (b) are under $P_{NO} = 1$, $P_{CO} = 1$. It is important to note that the coverage of $*$N is kept fixed by applying a potential of $-(\Delta G_{*N} - \Delta G_{*NO})/2e$ with Cu, Cu(110), and Cu(100) at 0.34, 0.29, and 0.27 V vs. RHE respectively. These potentials indicate that it is fair to not consider hydrocarbons formation from CO reduction where a much more negative potential is demanded (below -0.4 V vs. RHE).[19] Note that in supporting information heatmaps (Fig. S4) are presented at lower potentials, showing a clear decay in NO conversion towards urea with respect to potential. This is also observed in the experiment (Fig. 1). Our model demonstrates that the applied potential is a critical parameter for this NO + CO co-reduction. To be more specific, the potential needs to be inside a window where CO is present while NO reduction is enabled. This is observed as NH_3 and urea formation tracks each other in the experimental data (see Fig. 1). Furthermore, competition with the co-reduction takes place if the potential is increase further, so that CO reduction or HER begins to compete with the chemical C-N coupling step. In total the potential plays a vital role for the C-N coupling during NO + CO co-reduction, as also observed for N-N coupling[31] and C-C coupling.[34]

In Fig. 5(a), three regions can be classified in this model framework. Region (1) shows H_2 as a major product and region (2) represents urea production and NH_3 formation. Region (3) illustrates little activity for co-reduction of NO + CO due to unfavourable adsorption of NO and CO even though there are low activation barriers for $*$CO and $*$N coupling. In region (2), a higher rate (red area) can be obtained from a weakening $*$NO or $*$CO adsorption, although without having desorption. As for the formation of NH_3, our previous study has shown that

a stronger $*$NO relative to Cu is demanded in order to obtain a higher rate or FE.[24] As a result, a slightly weaker $*$NO adsorption relative to Cu, like Cu(100) in Fig. 5(b), not only improves selective urea production, but also promotes a high rate. This also hints that Cu alloys like CuAu may be promising for future experimental explorations. Additionally, shown in Fig. 5(b-d), our model shows that the selectivity of NO + CO co-reduction towards urea versus ammonia is enhanced via lowering the partial pressure of NO relative to CO. Using different nitrogen sources, as shown in Fig. 1, impacts not only the absolute urea formation rates but also the relative urea to ammonia formation. As our model currently relies on the observations in Shibata's experiments, it is highly relevant to reproduce those data in the near future to make the data and model valid. Notably, even quantifying urea versus ammonia can be a challenge to confirm sufficiently.

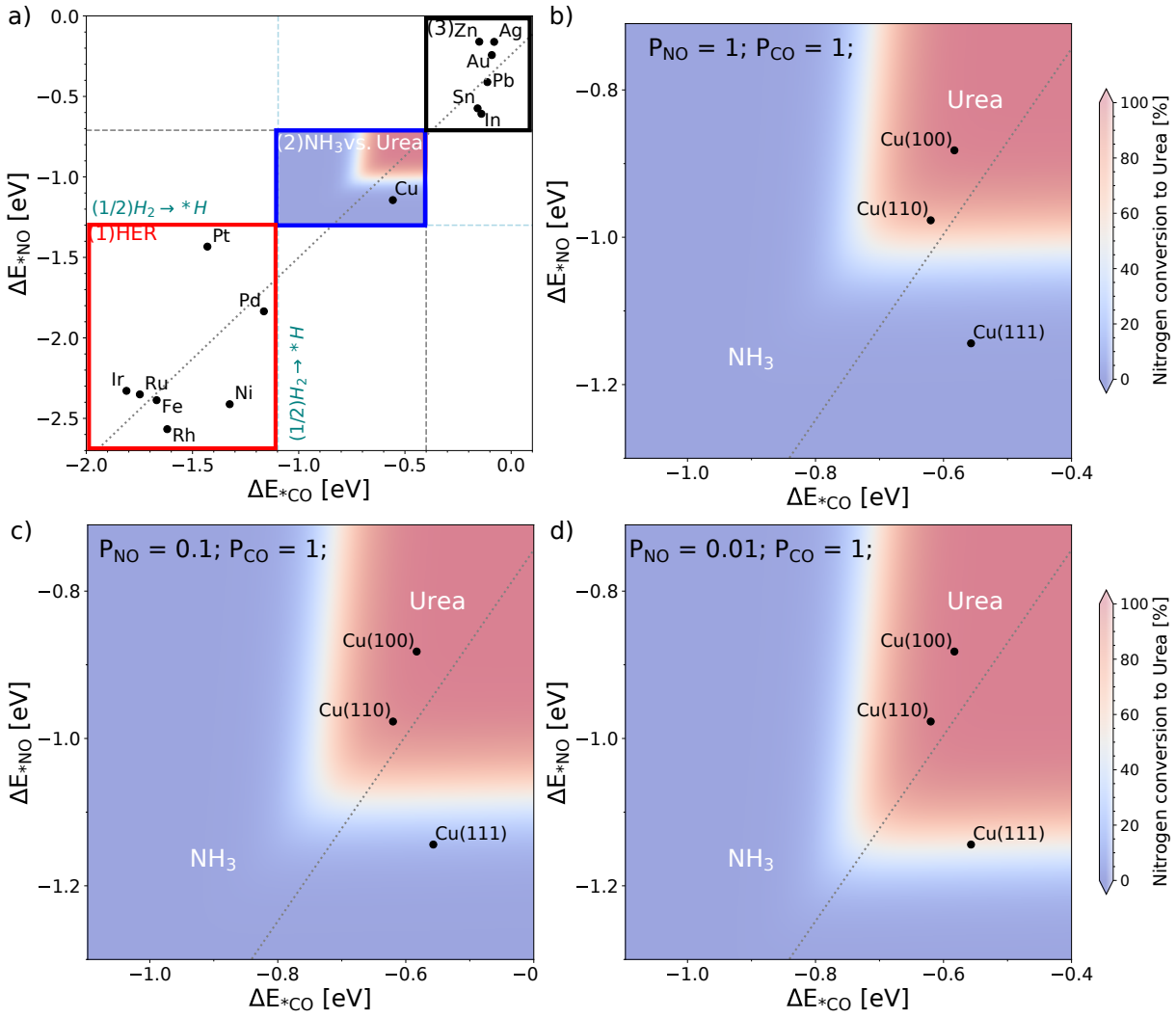

Figure 5: 2-D activity heatmap describing the nitrogen conversion for urea production as a function of ΔE_{*CO} and ΔE_{*NO}, computed at a temperature of 300K with (a) and (b) under $P_{NO} = 1$, $P_{CO} = 1$; (c) $P_{NO} = 0.1$, $P_{CO} = 1$; (d) $P_{NO} = 0.01$, $P_{CO} = 1$. The coverage of $*$N is kept fixed by applying a potential of -$(\Delta G_{*N} - \Delta G_{*NO})/2$ with Cu, Cu(110), and Cu(100) at 0.34, 0.29, and 0.27 V vs. RHE respectively. Here, $R_{urea}/(R_{urea} + R_{NH_3}) \times 100$ % equation has only been utilized in the area where $*$NO and $*$CO adsorbed but not binding $*$H. Region (1): Hydrogen evolution; Region (2): Urea and NH_3 production; Region (3): little activity. The gray dotted line is the linear fitting for $*$NO and $*$CO adsorption energies. It can be noted here Cu(100) not only benefits that the C-C coupling in CO reduction[39] but also favours C-N coupling during NO + CO co-reductions.

In this study, we use DFT simulations to investigate electrocatalytic NO + CO co-reduction over metal catalysts. Analogous to classifying CO_2 reduction by $*$CO vs. $*$H and NO reduction by $*$NO vs. $*$H, we utilize the classification scheme by plotting $*$NO vs. $*$CO.

Direct comparison of ∗NO vs. ∗CO shows that ∗NO binds stronger. Cu stands out with the unique property that it can bind both ∗NO and ∗CO but not having H_{upd}, leading to NO or CO reduction taking place prior to HER.

We show that C-N coupling is possible in the narrow window of ∗NO and ∗CO adsorbed but not binding ∗H. Among all the metals investigated here, Cu is predicted to be the most selective catalyst to produce urea. The results suggest that the key enabling steps on Cu in the formation of urea from co-reduction of NO + CO are first the hydrogenation of ∗NO and following the ∗CO + ∗N coupling. Firstly, if adsorbed ∗NOH can be stabilized relative to adsorbed ∗NO on Cu, the necessary overpotential can be reduced, which indicates a more efficient process. Besides, a relatively weaker ∗CO adsorption is needed in order to have a lower activation barrier for the coupling between ∗CO and ∗N. However, the hydrogenation of ∗NO is a shared limiting step both for urea and ammonia production, making a fundamental challenge in the formation of urea versus the conversion towards NH_3. This is also observed experimentally. These descriptor-based analysis in this work provides a description of NO + CO co-reduction or even CO_2 + NO_3^-/NO_2^- reduction network on metals at atomic scale. The results presented in the current study will form the basis of a search for improved understanding of the co-reduction of NO + CO on metals, suggesting a promising technology for amides especially urea formation. There are multiple opportunities and investigations required to understand these types of complicated reaction. Solvation effects could be investigated by implicit solvent and *ab initio* molecular dynamics.[40] We suggest for future work, to explore explicit dependence from pH,[40] applied potential,[40,41] surface coverages,[42] and ions from grand canonical DFT[41] for a more detailed understanding of C-N bond formation. Besides, as known from organic chemistry, other C-N formation, like C=N bond formation in oxime,[11] might be interesting to be investigated via this electrocatalytic process.

Supporting Information

Supplementary information for the computational details; Investigation of C-N couplings (Fig. S1-S3); The influence from applied potential on activity (Fig. S4).

Acknowledgement

We acknowledge support from the research grant 9455 from VILLUM FONDEN. The Center for High Entropy Alloys Catalysis is sponsored by the Danish National Research Foundation centers of excellence, Project DNRF149. A. Bagger acknowledges the Carlsberg foundation (CF21-0144).

References

(1) Davies, B. J. V.; Šarić, M.; Figueiredo, M. C.; Schjødt, N. C.; Dahl, S.; Moses, P. G.; Escudero-Escribano, M.; Arenz, M.; Rossmeisl, J. Electrochemically Generated Copper Carbonyl for Selective Dimethyl Carbonate Synthesis. *ACS Catal.* **2019**, *9*, 859–866, DOI: 10.1021/acscatal.8b03682.

(2) Jouny, M.; Lv, J.-J.; Cheng, T.; Ko, B. H.; Zhu, J.-J.; Goddard, W. A., 3rd; Jiao, F. Formation of carbon-nitrogen bonds in carbon monoxide electrolysis. *Nat. Chem.* **2019**, *11*, 846–851, DOI: 10.1038/s41557-019-0312-z.

(3) Chen, C.; Zhu, X.; Wen, X.; Zhou, Y.; Zhou, L.; Li, H.; Tao, L.; Li, Q.; Du, S.; Liu, T.; Yan, D.; Xie, C.; Zou, Y.; Wang, Y.; Chen, R.; Huo, J.; Li, Y.; Cheng, J.; Su, H.; Zhao, X.; Cheng, W.; Liu, Q.; Lin, H.; Luo, J.; Chen, J.; Dong, M.; Cheng, K.; Li, C.; Wang, S. Coupling N2 and CO2 in H2O to synthesize urea under ambient conditions. *Nat. Chem.* **2020**, *12*, 717–724, DOI: 10.1038/s41557-020-0481-9.

(4) Sabatini, M. T.; Boulton, L. T.; Sneddon, H. F.; Sheppard, T. D. A green chem-

istry perspective on catalytic amide bond formation. *Nat. Catal.* **2019**, *2*, 10–17, DOI: 10.1038/s41929-018-0211-5.

(5) Lv, Z.-J.; Wei, J.; Zhang, W.-X.; Chen, P.; Deng, D.; Shi, Z.-J.; Xi, Z. Direct transformation of dinitrogen: synthesis of N-containing organic compounds via N-C bond formation. *Natl. Sci. Rev.* **2020**, *7*, 1564–1583, DOI: 10.1093/nsr/nwaa142.

(6) Tang, C.; Zheng, Y.; Jaroniec, M.; Qiao, S.-Z. Electrocatalytic Refinery for Sustainable Production of Fuels and Chemicals. *Angew. Chem. Int. Ed. 60*, 19572–19590, DOI: 10.1002/anie.202101522.

(7) Giddey, S.; Badwal, S.; Kulkarni, A. Review of electrochemical ammonia production technologies and materials. *Int. J. Hydrogen Energy* **2013**, *38*, 14576–14594, DOI: 10.1016/j.ijhydene.2013.09.054.

(8) Qiao, J.; Liu, Y.; Hong, F.; Zhang, J. A review of catalysts for the electroreduction of carbon dioxide to produce low-carbon fuels. *Chem. Soc. Rev.* **2014**, *43*, 631–675, DOI: 10.1039/C3CS60323G.

(9) Aresta, M.; Dibenedetto, A.; Angelini, A. Catalysis for the Valorization of Exhaust Carbon: from CO2 to Chemicals, Materials, and Fuels. Technological Use of CO2. *Chem. Rev.* **2014**, *114*, 1709–1742, DOI: 10.1021/cr4002758.

(10) Huang, Y.; Yang, R.; Wang, C.; Meng, N.; Shi, Y.; Yu, Y.; Zhang, B. Direct Electrosynthesis of Urea from Carbon Dioxide and Nitric Oxide. *ACS Energy Lett.* **2022**, *7*, 284–291, DOI: 10.1021/acsenergylett.1c02471.

(11) Zhang, X.; Jing, H.; Chen, S.; Liu, B.; Yu, L.; Xiao, J.; Deng, D. Direct electrosynthesis of valuable C=N compound from NO. *Chem Catalysis* **2022**, *2*, 1807–1818, DOI: 10.1016/j.checat.2022.06.003.

(12) Kim, J. E.; Choi, S.; Balamurugan, M.; Jang, J. H.; Nam, K. T. Electrochemical C-N Bond Formation for Sustainable Amine Synthesis. *Trends in Chemistry* **2020**, *2*, 1004–1019, DOI: 10.1016/j.trechm.2020.09.003.

(13) Shibata, M.; Yoshida, K.; Furuya, N. Electrochemical synthesis of urea on reduction of carbon dioxide with nitrate and nitrite ions using Cu-loaded gas-diffusion electrode. *J. Electroanal. Chem.* **1995**, *387*, 143–145, DOI: 10.1016/0022-0728(95)03992-P.

(14) Liu, X.; Jiao, Y.; Zheng, Y.; Jaroniec, M.; Qiao, S. Mechanism of C-N bonds formation in electrocatalytic urea production revealed by ab initio molecular dynamics simulation. *Nat. Commun.* **2022**, *13*, 5471, DOI: 10.1038/s41467-022-33258-0.

(15) Shibata, M.; Yoshida, K.; Furuya, N. Electrochemical Synthesis of Urea at Gas-Diffusion Electrodes: IV. Simultaneous Reduction of Carbon Dioxide and Nitrate Ions with Various Metal Catalysts. *J. Electrochem. Soc.* **1998**, *145*, 2348–2353, DOI: 10.1149/1.1838641.

(16) Shibata, M.; Yoshida, K.; Furuya, N. Electrochemical synthesis of urea at gas-diffusion electrodes: Part II. Simultaneous reduction of carbon dioxide and nitrite ions at Cu, Ag and Au catalysts. *J. Electroanal. Chem.* **1998**, *442*, 67–72, DOI: 10.1016/S0022-0728(97)00504-4.

(17) Higgins, D.; Hahn, C.; Xiang, C.; Jaramillo, T. F.; Weber, A. Z. Gas-Diffusion Electrodes for Carbon Dioxide Reduction: A New Paradigm. *ACS Energy Lett.* **2019**, *4*, 317–324, DOI: 10.1021/acsenergylett.8b02035.

(18) Möller, T.; Ngo Thanh, T.; Wang, X.; Ju, W.; Jovanov, Z.; Strasser, P. The product selectivity zones in gas diffusion electrodes during the electrocatalytic reduction of CO2. *Energy Environ. Sci.* **2021**, 5995–6006, DOI: 10.1039/D1EE01696B.

(19) Hori, Y.; Wakebe, H.; Tsukamoto, T.; Koga, O. Electrocatalytic process of CO se-

lectivity in electrochemical reduction of CO2 at metal electrodes in aqueous media. *Electrochimica Acta* **1994**, *39*, 1833–1839, DOI: 10.1016/0013-4686(94)85172-7.

(20) Nitopi, S.; Bertheussen, E.; Scott, S. B.; Liu, X.; Engstfeld, A. K.; Horch, S.; Seger, B.; Stephens, I. E. L.; Chan, K.; Hahn, C.; Nørskov, J. K.; Jaramillo, T. F.; Chorkendorff, I. Progress and Perspectives of Electrochemical CO2 Reduction on Copper in Aqueous Electrolyte. *Chem. Rev.* **2019**, *119*, 7610–7672, DOI: 10.1021/acs.chemrev.8b00705.

(21) Wang, Y.; Zhou, W.; Jia, R.; Yu, Y.; Zhang, B. Unveiling the Activity Origin of a Copper-based Electrocatalyst for Selective Nitrate Reduction to Ammonia. *Angew. Chem. Int. Ed.* **2020**, *59*, 5350–5354, DOI: 10.1002/anie.201915992.

(22) Wang, Y.; Xu, A.; Wang, Z.; Huang, L.; Li, J.; Li, F.; Wicks, J.; Luo, M.; Nam, D.-H.; Tan, C.-S.; Ding, Y.; Wu, J.; Lum, Y.; Dinh, C.-T.; Sinton, D.; Zheng, G.; Sargent, E. H. Enhanced Nitrate-to-Ammonia Activity on Copper-Nickel Alloys via Tuning of Intermediate Adsorption. *J. Am. Chem. Soc.* **2020**, *142*, 5702–5708, DOI: 10.1021/jacs.9b13347.

(23) Long, J.; Chen, S.; Zhang, Y.; Guo, C.; Fu, X.; Deng, D.; Xiao, J. Direct Electrochemical Ammonia Synthesis from Nitric Oxide. *Angew. Chem., Int. Ed.* **2020**, *59*, 9711–9718, DOI: doi.org/10.1002/anie.202002337.

(24) Wan, H.; Bagger, A.; Rossmeisl, J. Electrochemical Nitric Oxide Reduction on Metal Surfaces. *Angew. Chem. Int. Ed.* **2021**, *60*, 21966–21972, DOI: 10.1002/anie.202108575.

(25) Rosca, V.; Duca, M.; de Groot, M. T.; Koper, M. T. M. Nitrogen Cycle Electrocatalysis. *Chem. Rev.* **2009**, *109*, 2209–2244, DOI: 10.1021/cr8003696.

(26) Duca, M.; Koper, M. T. M. Powering denitrification: the perspectives of electrocatalytic nitrate reduction. *Energy Environ. Sci.* **2012**, *5*, 9726–9742, DOI: 10.1039/C2EE23062C.

(27) Duca, M.; van der Klugt, B.; Koper, M. Electrocatalytic reduction of nitrite on transition and coinage metals. *Electrochim. Acta* **2012**, *68*, 32–43, DOI: 10.1016/j.electacta.2012.02.037.

(28) Garcia-Segura, S.; Lanzarini-Lopes, M.; Hristovski, K.; Westerhoff, P. Electrocatalytic reduction of nitrate: Fundamentals to full-scale water treatment applications. *Appl. Catal. B* **2018**, *236*, 546–568, DOI: 10.1016/j.apcatb.2018.05.041.

(29) Anastasiadou, D.; van Beek, Y.; Hensen, E. J. M.; Costa Figueiredo, M. Ammonia electrocatalytic synthesis from nitrate. *Electrochem. Sci. Adv.* e2100220, DOI: 10.1002/elsa.202100220.

(30) Mou, T.; Wang, Y.; Deák, P.; Li, H.; Long, J.; Fu, X.; Zhang, B.; Frauenheim, T.; Xiao, J. Predictive Theoretical Model for the Selective Electroreduction of Nitrate to Ammonia. *J. Phys. Chem. Lett.* **2022**, *13*, 9919–9927, DOI: 10.1021/acs.jpclett.2c02452, PMID: 36256962.

(31) Long, J.; Guo, C.; Fu, X.; Jing, H.; Qin, G.; Li, H.; Xiao, J. Unveiling Potential Dependence in NO Electroreduction to Ammonia. *J.Phys. Chem. Lett.* **2021**, *12*, 6988–6995, DOI: 10.1021/acs.jpclett.1c01691.

(32) Bagger, A.; Ju, W.; Varela, A. S.; Strasser, P.; Rossmeisl, J. Electrochemical CO2 Reduction: A Classification Problem. *ChemPhysChem* **2017**, *18*, 3266–3273, DOI: 10.1002/cphc.201700736.

(33) Wan, H.; Jiao, Y.; Bagger, A.; Rossmeisl, J. Three-Dimensional Carbon Electrocatalysts for CO2 or CO Reduction. *ACS Catal.* **2021**, *11*, 533–541, DOI: 10.1021/acscatal.0c04878.

(34) Raaijman, S. J.; Schellekens, M. P.; Corbett, P. J.; Koper, M. T. M. High-Pressure CO Electroreduction at Silver Produces Ethanol and Propanol. *Angew. Chem. Int. Ed.* **2021**, *60*, 21732–21736, DOI: 10.1002/anie.202108902.

(35) Nørskov, J. K.; Studt, F.; Abild-Pedersen, F.; Bligaard, T. *Fundamental concepts in heterogeneous catalysis*; Wiley: Hoboken New Jersey, 2014; p 57.

(36) Schouten, K. J. P.; Qin, Z.; Pérez Gallent, E.; Koper, M. T. M. Two Pathways for the Formation of Ethylene in CO Reduction on Single-Crystal Copper Electrodes. *J. Am. Chem. Soc.* **2012**, *134*, 9864–9867, DOI: 10.1021/ja302668n.

(37) Verdaguer-Casadevall, A.; Li, C. W.; Johansson, T. P.; Scott, S. B.; McKeown, J. T.; Kumar, M.; Stephens, I. E. L.; Kanan, M. W.; Chorkendorff, I. Probing the Active Surface Sites for CO Reduction on Oxide-Derived Copper Electrocatalysts. *J. Am. Chem. Soc.* **2015**, *137*, 9808–9811, DOI: 10.1021/jacs.5b06227.

(38) Cao, N.; Quan, Y.; Guan, A.; Yang, C.; Ji, Y.; Zhang, L.; Zheng, G. Oxygen vacancies enhanced cooperative electrocatalytic reduction of carbon dioxide and nitrite ions to urea. *J. Colloid Interface Sci.* **2020**, *577*, 109–114, DOI: 10.1016/j.jcis.2020.05.014.

(39) Bagger, A.; Arnarson, L.; Hansen, M. H.; Spohr, E.; Rossmeisl, J. Electrochemical CO Reduction: A Property of the Electrochemical Interface. *J. Am. Chem. Soc.* **2019**, *141*, 1506–1514, DOI: 10.1021/jacs.8b08839.

(40) Rossmeisl, J.; Jensen, K. D.; Petersen, A. S.; Arnarson, L.; Bagger, A.; Escudero-Escribano, M. Realistic Cyclic Voltammograms from Ab Initio Simulations in Alkaline and Acidic Electrolytes. *J. Phys. Chem. C* **2020**, *124*, 20055–20065, DOI: 10.1021/acs.jpcc.0c04367.

(41) Melander, M. M.; Kuisma, M. J.; Christensen, T. E. K.; Honkala, K. Grand-canonical approach to density functional theory of electrocatalytic systems: Thermodynamics of solid-liquid interfaces at constant ion and electrode potentials. *J. Chem. Phys.* **2019**, *150*, 041706, DOI: 10.1063/1.5047829.

(42) Groß, A.; Sakong, S. Ab Initio Simulations of Water/Metal Interfaces. *Chem. Rev.* **2022**, *122*, 10746–10776, DOI: 10.1021/acs.chemrev.1c00679.

Graphical TOC Entry

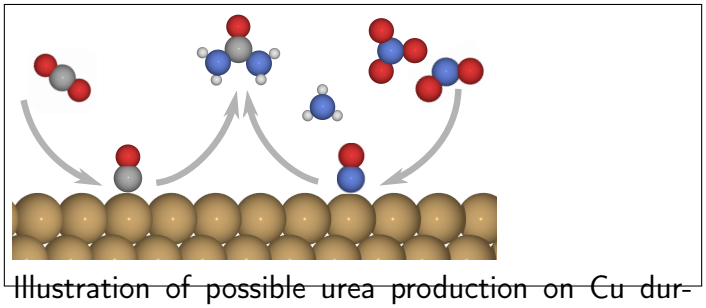

Illustration of possible urea production on Cu during electrocatalytic co-reduction of nitric oxide and carbon monoxide